

Probing Nuclear Geometry through Multi-Particle Azimuthal Correlations and Rapidity-Even Dipolar Flow in $^{16}\text{O}+^{16}\text{O}$ Collisions

Kaiser Shafi* and Sandeep Chatterjee†

*Department of Physical Sciences,
Indian Institute of Science Education and Research Berhampur,
Laudigam-760003, Dist.-Ganjam, Odisha, India*

(Dated: June 9, 2025)

We study symmetric and asymmetric cumulants as well as rapidity-even dipolar flow in $^{16}\text{O}+^{16}\text{O}$ collisions at $\sqrt{s_{NN}} = 200$ GeV to explore α -clustering phenomena in light nuclei within the viscous relativistic hydrodynamics framework. Signatures of α -clustering manifest in the anisotropic flow coefficients and their correlations—particularly in observables involving elliptic-triangular flow correlations. We show that final-state symmetric and asymmetric cumulants—especially NSC(2, 3) and NAC_{2,1}(2, 3)—are sensitive to the initial nuclear geometry. Additionally, we observe a significant difference in rapidity-even dipolar flow, v_1^{even} , between α -clustered and Woods-Saxon configurations in high-multiplicity events. These findings underscore the pivotal role of nuclear structure in heavy-ion collision dynamics and provide observables for distinguishing nuclear geometries, particularly in ultra-central collisions.

I. INTRODUCTION

The study of nuclear geometry has long been essential for understanding the structure and dynamics of atomic nuclei. Evidence for nuclear deformation is generally derived from low-energy spectroscopic measurements and models that assess reduced transition probabilities between low-lying rotational states, utilizing beam energies below a few tens of MeV per nucleon [1–3]. This focus on nuclear structure has provided insights into the fundamental forces and interactions that govern matter at the subatomic level [4], with ongoing challenges in investigating complex nucleon-nucleon interactions at low energies [5, 6]. As part of this, various phenomenological models [6–10] and experimental methodologies [11–13] have been developed, exploring nuclei such as oxygen and neon through advanced approaches like NLEFT simulations [14, 15], PGCM [16–18], and VMC [19].

In high-energy nuclear physics, one key motivation is to probe the bulk properties of QCD matter under extreme conditions, such as those found in the early universe or in astrophysical objects [20]. A significant example is the quark-gluon plasma (QGP), a hot phase of QCD matter that behaves as a near-perfect fluid [21]. The QGP provides a unique environment for studying the collective behavior of strongly interacting matter, and its properties are inferred from the harmonic spectrum of the azimuthal distributions of final-state hadrons. The coefficients v_n associated with these distributions quantify anisotropic flow and serve as direct signatures of hydrodynamic behavior, offering critical insights into the early dynamics of the collision [22, 23]. Understanding of QGP has been central to high-energy nuclear physics, with key experimental results from RHIC and the LHC providing

valuable insights into its properties under extreme conditions [24–29]. These findings support the widely accepted model describing the hydrodynamic expansion of QGP with low shear viscosity [30–32] and a subsequent late-stage hadronic afterburner for interactions among hadrons.

A unique aspect of relativistic heavy-ion collisions is their ability to probe the initial geometric structures of the colliding nuclei. These collisions provide important information about the spatial distribution and clustering of nucleons within light nuclei, which can be studied through observables like collective flow [33–51], Hanbury Brown-Twiss (HBT) correlations [52–54], and fluctuations [55, 56]. These observables shed light on the initial nuclear geometry, offering valuable clues regarding the properties of the initial-state nuclei, and are essential tools for investigating nuclear structure at high energies. In recent decades, relativistic heavy-ion collisions have become a crucial technique for probing the intrinsic properties of nuclei, including their geometric configurations and cluster structures [57–67].

The dynamics of nuclear collisions are now widely understood through the framework of relativistic hydrodynamics, where the collective behavior of the system is driven by the initial collision geometry [23, 68–75]. Precision observables for probing the hydrodynamic evolution of these collisions, such as multi-particle correlations [76–78], soft-hard multi-particle azimuthal correlations [73, 79, 80], have become increasingly important in recent years, driving the field into a new era of precision physics [81–85].

A. Symmetric and Asymmetric Cumulants of Flow Amplitudes

Anisotropies observed in the momentum distributions of produced particles carry information about the QGP properties [20, 30, 86]. After hadronization, particles are

* kaisers@iiserbpr.ac.in

† sandeep@iiserbpr.ac.in

emitted anisotropically in the transverse plane, quantified using Fourier series of flow amplitudes v_n and symmetry planes ψ_n [87],

$$\frac{dN}{d\phi} = \frac{1}{2\pi} \left[1 + 2 \sum_{n=1}^{\infty} v_n \cos[n(\phi - \psi_n)] \right] \quad (1)$$

Collective flow provides insight into the QGP medium [30, 88, 89]. The impact parameter driven spatial geometry of the fireball and nucleonic fluctuations lead to various anisotropic flow harmonics. The second-order elliptic flow (v_2) originates from the geometry of the overlap region [90–96], while the third-order triangular flow (v_3) arises from event-by-event nucleon and sub-nucleon fluctuations [35, 97–100]. These flow harmonics are sensitive to the equation of state (EoS) and transport properties of the fireball, such as viscosity [101–105].

Recent studies have demonstrated that higher-order observables, such as flow cumulants, provide valuable insights into the properties of the Quark-Gluon Plasma (QGP) by probing genuine correlations between different moments of flow harmonics while remaining robust against non-flow effects, as evidenced by simulations using the HIJING Monte Carlo generator [106]. These developments stem from advancements in multi-particle correlation analysis, which have enabled the assessment of correlators involving different harmonics [76, 107–109]. Symmetric and asymmetric cumulants, in particular, have emerged as a powerful tools for quantifying correlations between event-by-event fluctuations in flow harmonics v_m and v_n , allowing for the differentiation of true collective flow from non-flow contributions. Measurements by the STAR and the ALICE collaborations have revealed significant correlations among v_2 , v_3 , and v_4 , and have shown sensitivity to the shear viscosity of the medium [35, 97–100].

The symmetric cumulant, $SC(m, n)$, is defined as [107]

$$\begin{aligned} SC(m, n) &\equiv \langle \langle \cos(m\varphi_1 + n\varphi_2 - m\varphi_3 - n\varphi_4) \rangle \rangle_c \\ &= \langle \langle \cos(m\varphi_1 + n\varphi_2 - m\varphi_3 - n\varphi_4) \rangle \rangle \\ &\quad - \langle \langle \cos[m(\varphi_1 - \varphi_2)] \rangle \rangle \langle \langle \cos[n(\varphi_1 - \varphi_2)] \rangle \rangle \\ &\equiv \langle v_m^2 v_n^2 \rangle_c = \langle v_m^2 v_n^2 \rangle - \langle v_m^2 \rangle \langle v_n^2 \rangle \end{aligned} \quad (2)$$

The subscript c denotes that this quantity is a cumulant. A positive or negative value for $SC(m, n)$ indicates whether there is a correlation or anti-correlation between v_m^2 and v_n^2 . Specifically, when v_m^2 exceeds its average value in an event, the chances that v_n^2 similarly exceeds its average value rise (or fall) accordingly. This focus on correlations across different flow harmonics enables effective comparisons between experimental results and theoretical predictions.

To mitigate the influence of the magnitudes of v_m and v_n on the symmetric cumulant value, $SC(m, n)$ is normalized using their average values, $\langle v_m^2 \rangle$ and $\langle v_n^2 \rangle$. This normalization leads to what is termed the normalized symmetric cumulant, $NSC(m, n)$, facilitating straightforward comparisons of experimental data with theoretical

models as well as between initial and final state fluctuations [108]. The normalized symmetric cumulant, $NSC(m, n)$, is given by [110]:

$$NSC(m, n) = \frac{SC(m, n)}{\langle v_m^2 \rangle \langle v_n^2 \rangle} \quad (3)$$

Asymmetric cumulants capture genuine correlations between different moments of flow harmonics. The asymmetric cumulant, $AC_{2,1}(m, n)$, is defined as [106]:

$$\begin{aligned} AC_{2,1}(m, n) &\equiv \langle \langle e^{i(m\varphi_1 + m\varphi_2 + n\varphi_3 - m\varphi_4 - m\varphi_5 - n\varphi_6)} \rangle \rangle_c \\ &= \langle \langle e^{i(m\varphi_1 + m\varphi_2 + n\varphi_3 - m\varphi_4 - m\varphi_5 - n\varphi_6)} \rangle \rangle \\ &\quad - \langle \langle e^{i(m\varphi_1 + m\varphi_2 - m\varphi_3 - m\varphi_4)} \rangle \rangle \langle \langle e^{i(n\varphi_1 - n\varphi_2)} \rangle \rangle \\ &\quad - 2 \langle \langle e^{i(m\varphi_1 + n\varphi_2 - m\varphi_3 - n\varphi_4)} \rangle \rangle \langle \langle e^{i(m\varphi_1 - m\varphi_2)} \rangle \rangle \\ &\quad + 2 \langle \langle e^{i(m\varphi_1 - m\varphi_2)} \rangle \rangle^2 \langle \langle e^{i(n\varphi_1 - n\varphi_2)} \rangle \rangle \\ &\equiv \langle (v_m^2)^2 v_n^2 \rangle_c = \langle v_m^4 v_n^2 \rangle - \langle v_m^4 \rangle \langle v_n^2 \rangle \\ &\quad - 2 \langle v_m^2 v_n^2 \rangle \langle v_m^2 \rangle + 2 \langle v_m^2 \rangle^2 \langle v_n^2 \rangle \end{aligned} \quad (4)$$

In this equation, the subscripts (2, 1) signify the powers of v_m^2 and v_n^2 in the cumulant $\langle (v_m^2)^2 v_n^2 \rangle_c$. These equations denote genuine multivariate cumulants. Additionally, the asymmetric cumulant $AC_{1,1}(m, n)$ equates to the symmetric cumulant $SC(m, n)$, highlighting a broader application of the asymmetric cumulants. The normalization of these cumulants provides significant advantages, such as facilitating meaningful comparisons of results and allowing for the identification of initial state effects and changes resulting from hydrodynamic evolution. Since the scales of AC predictions differ between initial and final states, normalization aids in reconciling these disparities. Moreover, as flow amplitudes vary with transverse momentum (p_T), normalization negates the p_T dependence present in linear combinations of these amplitudes, like symmetric and asymmetric cumulants, thus enabling comparisons across different models and data sets with a range of p_T values.

$$NAC_{2,1}(m, n) = \frac{AC_{2,1}(m, n)}{\langle v_m^2 \rangle^2 \langle v_n^2 \rangle} \quad (5)$$

We computed both normalized symmetric and asymmetric cumulants for $^{16}\text{O} + ^{16}\text{O}$ collisions at $\sqrt{s_{NN}} = 200$ GeV. Previous studies have explored these cumulants in heavy-ion collisions, such as Au+Au and Pb+Pb, employing various hydrodynamic and hadronic transport models [108, 110–117]. Additionally, experiments conducted by the STAR experiment at RHIC [118] and the ALICE experiment at LHC [119, 120] have measured these cumulants. The ALICE collaboration has performed a systematic study of $SC(m, n)$ and $NSC(m, n)$ [109]. Their findings show a positive correlation between v_2 and v_4 , while indicating a negative correlation between v_2 and v_3 . In addition to symmetric and asymmetric cumulants, various other correlators have also been studied [121–124].

B. v_1^{even}

Directed flow can be characterized as either rapidity-even or rapidity-odd [125]. The odd component, $v_1^{\text{odd}}(y)$, originating from the geometry of the overlap region of the collision and associated with the reaction plane, has been extensively studied [126–138]. In symmetric collisions, the even component, $v_1^{\text{even}}(y)$, arises from fluctuations in the initial nucleon positions and varies weakly with rapidity [139, 140]. These fluctuations break the symmetry of the initial density profile and generate a preferred direction, where the gradient is steepest. This anisotropy in the initial state is quantified by the dipole asymmetry:

$$\varepsilon_1 e^{i\Phi_1} = -\frac{\langle r^3 e^{i\phi} \rangle}{\langle r^3 \rangle}, \quad (6)$$

where the averages are taken over the initial transverse entropy density profile, with (r, ϕ) as polar coordinates centered such that $\langle r e^{i\phi} \rangle = 0$. Experimentally, v_1 is extracted from a two-particle correlation, which scales like $(v_1)^2$, so the measured v_1 should scale with the root-mean-square (rms) dipole asymmetry, $\varepsilon_1\{2\} \equiv \sqrt{\langle \varepsilon_1^2 \rangle}$ [141]. Due to fluctuations, ε_1 is non-zero even at midrapidity. Hydrodynamic expansion of the dipole asymmetry, ε_1 , generates directed flow anisotropy in the momentum distribution of the emitted particles. High- p_T particles are preferentially emitted in the direction of the steepest gradient (Ψ_1), where the fluid velocity is the largest [142]. This anisotropy is characterized by the directed flow with respect to Ψ_1 :

$$v_1 = \langle \cos(\phi - \Psi_1) \rangle, \quad (7)$$

where ϕ is the particle azimuthal angle, and the average is taken over particles in each event. Because total transverse momentum must approximately vanish, high- p_T particles with positive v_1 imply a corresponding negative v_1 for low- p_T particles, resulting in a characteristic p_T -dependence of v_1 [23].

Rapidity even directed flow is typically analyzed via the event-plane method, analogous to that used for elliptic flow [143, 144]. In each event, the event plane angle Ψ_1 is defined as [145]:

$$Q e^{i\Psi_1} = \sum_j w_j e^{i\phi_j},$$

where the sum runs over charged particles in an event. The weight w_j for each particle is selected such that $\langle w p_T \rangle = 0$ to prevent bias from momentum conservation, as these correlations are proportional to p_T [146, 147]. For the even component, the weight is chosen to depend on p_T , as follows [145]:

$$w(p_T) = p_T - \frac{\langle p_T^2 \rangle}{\langle p_T \rangle},$$

where the inner average is over particles in an event, and the outer over all events. This choice satisfies $\langle w p_T \rangle = 0$,

suppressing momentum conservation bias. The final Q -weighted directed flow coefficient is given by:

$$v_1^{\text{even}} = \frac{\langle Q \cos(\phi - \Psi_1) \rangle}{\sqrt{\langle Q^2 \rangle}}.$$

The Fourier harmonics v_n probe increasingly smaller spatial scales with larger n , making higher harmonics more sensitive to viscosity. In contrast, v_1 is relatively insensitive to viscous effects [148–151], and its proportionality to ε_1 makes it a direct probe of the system's early-time dipole asymmetry [152]. Measurements of v_1^{even} have been reported in Au+Au collisions by the STAR Collaboration at RHIC [153], and in Pb+Pb collisions by the ALICE and ATLAS Collaborations at the LHC [131, 146].

II. FRAMEWORK

In this work, we utilize a multi-component framework to simulate different stages of heavy ion collisions. The initial energy density profiles are generated using the TRENTo model. We compute the nuclear distribution using the three-parameter Fermi (3pF) distribution and tetrahedral configurations of α clusters (with different compactness of the α clusters in the nuclei) with the root-mean-square radius for ^{16}O kept constant. The 3pF nuclear distribution is given by:

$$\rho = \rho_0 (1 + \omega r^2/R^2) [1 + \exp((r - R)/a)]^{-1},$$

In the tetrahedral configurations, the shape of the oxygen nucleus is described by a tetrahedron with side length l , and the centers of the four α clusters are positioned at the vertices of the tetrahedron. The spatial coordinates of the nucleons in each α cluster are sampled from a 3D Gaussian distribution with a parameter r_α , which represents the root-mean-square radius of each cluster. The parameter r_α reflects the compactness of the α cluster in the nucleus: a smaller value of r_α corresponds to a denser cluster.

In this study, the nuclear density of ^{16}O is constructed using three different values of r_α , taken from the reference [154], to comprehensively understand the effect of α cluster configurations on the final observables. We impose that the root-mean-square radius of ^{16}O should be the same for the different densities, i.e.,

$$\sqrt{\langle r^2 \rangle} \equiv \sqrt{\frac{3l^2}{8} + r_\alpha^2} = 2.73 \text{ fm},$$

which is taken from nuclear structure experiments [155]. The differences between charge density and nuclear mass density are ignored. In the case of a more compact α cluster, a larger value of l is required. At small values of r_α/l , distinct configurations of hotspots—three at the vertices of a triangle, with a fourth at the center—emerge. The nuclear distribution parameters are listed in Table I, and

TABLE I. The parameters [155] for the nuclear distributions of ^{16}O with Woods–Saxon and tetrahedral configurations of α clusters.

	Distribution	R	a	ω
WS	Woods–Saxon	2.608 fm	0.513 fm	-0.051
		l	r_α	r_α/l
Cl. I	α cluster	3.0	2.0	0.67
Cl. II	α cluster	3.6	1.6	0.44
Cl. III	α cluster	4.0	1.2	0.30

TABLE II. TRENTo model parameters used for $^{16}\text{O}+^{16}\text{O}$ collisions, taken from Refs. [44, 156].

Parameters	p	k	w_c	d_{\min}
Value	0.0	1.0	0.51 fm	0.4 fm

the two-dimensional density profiles, projected into the transverse plane of the collision, are shown in Fig. 1.

The parameters—reduced thickness parameter (p), gamma distribution shape parameter (k), nucleon width (w_c), and minimum nucleon-nucleon distance (d_{\min}), in TRENTo model for the simulation of $^{16}\text{O}+^{16}\text{O}$ collisions at $\sqrt{s_{NN}} = 200$ GeV are given in Table II.

The evolution of the energy-momentum tensor starts at an initial time of $\tau_0 = 0.4$ fm. The hydrodynamic equations are solved using the MUSIC code [157–160], which employs the Kurganov-Tadmor algorithm. We set a constant effective shear viscosity to entropy density ratio $\eta/s = 0.08$, calibrated to match the measured anisotropic flow coefficients of charged hadrons in Au+Au collisions at the same collision energy. A detailed

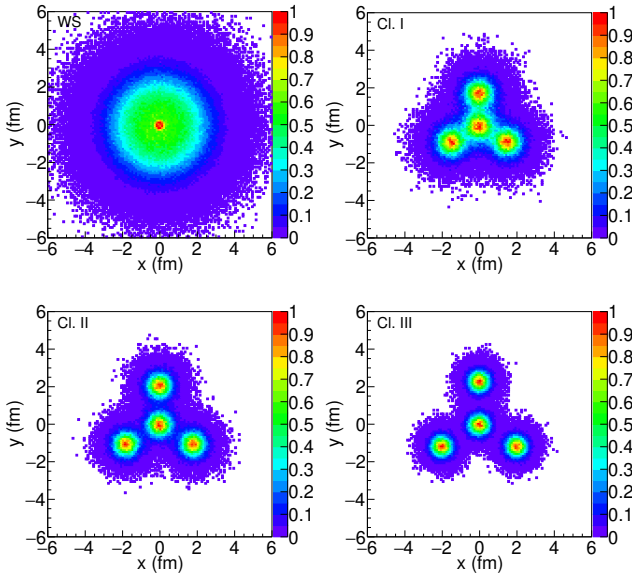


FIG. 1. Nuclear distributions of ^{16}O using Woods–Saxon and tetrahedral α -cluster configurations (see Table I).

TABLE III. Values of the transport coefficients used in the simulations for the different parameter sets.

Parameter Sets	η/s	ζ/s
I	0.08	0
II	0.12	0
III	0.08	$\zeta/s(T)$

description of the chosen parameters' values is available in Refs. [44, 156]. The specific bulk viscosity is treated as a temperature-dependent quantity and is parametrized as:

$$\frac{\zeta}{s} = \begin{cases} \lambda_1 e^{-(x-1)/\sigma_1} + \lambda_2 e^{-(x-1)/\sigma_2} + 0.001 & \text{for } T > 1.05T_C, \\ \lambda_3 e^{(x-1)/\sigma_3} + \lambda_4 e^{(x-1)/\sigma_4} + 0.03 & \text{for } T < 0.995T_C, \end{cases} \quad (8)$$

where $x = T/T_C$. The parameters $\lambda_1 = \lambda_3 = 0.9$, $\lambda_2 = 0.25$, $\lambda_4 = 0.22$, $\sigma_1 = 0.025$, $\sigma_2 = 0.13$, $\sigma_3 = 0.0025$, and $\sigma_4 = 0.022$ are fitted as described in [161].

For the equation of state (EoS), we employ the NEoS-B model [162], which is based on continuum-extrapolated lattice calculations at zero net baryon chemical potential [163–165] and smoothly matched to a hadron resonance gas EoS in the temperature range between 110 and 130 MeV [166].

For each nuclear configuration of ^{16}O , we performed hydrodynamic evolution on 5000 initial conditions for each of the centrality classes: 0-0.1%, 0-1%, 0-5%, 20-30%, and 40-50%, using two distinct parameter sets (Table III) for the simulations. A freeze-out hypersurface was constructed at a constant energy density of $\epsilon_f = 0.26$ GeV/fm³, corresponding to a local temperature of approximately 151 MeV. We calculate the invariant single-particle momentum distribution using the Cooper-Frye prescription [167] applied to this hypersurface which is continuous and does not require sampling, unless modeling subsequent late-stage hadronic interactions, the effects of which we also discuss. As a result, there are no fluctuations due to finite multiplicity, and no statistical error arises from hadronization. This approach allows for achieving reasonable statistical accuracy with a much smaller number of events compared to typical experiments [125]. From this distribution, we compute observables such as flow coefficients and mean transverse momentum. Finally, we compute both symmetric and asymmetric cumulants from the flow magnitudes.

The normalized symmetric cumulants, $\text{NSC}(m, n)$, normalized asymmetric cumulants, $\text{NAC}_{2,1}(m, n)$, and rapidity-even dipolar flow, v_1^{even} , are computed using pseudorapidity (η) ranges of $[-0.5, 0.5]$ and transverse momentum (p_T) ranges of $[0.01, 3.0]$ GeV. Statistical uncertainties for ensemble-level observables were estimated using the bootstrap method with resampling, which provides a robust estimate of sampling variance without relying on analytical error propagation.

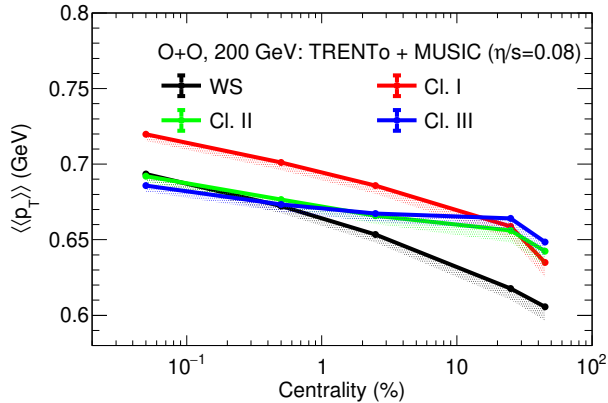


FIG. 2. $\langle\langle p_T \rangle\rangle$ in $^{16}\text{O}+^{16}\text{O}$ collisions at $\sqrt{s_{NN}} = 200$ GeV for the TRENTo+MUSIC framework. Band represents the systematics due to η/s .

III. RESULTS

A. Mean transverse momentum

Figure 2 shows how the average transverse momentum, $\langle\langle p_T \rangle\rangle$, varies with centrality in $^{16}\text{O}+^{16}\text{O}$ collisions. In relativistic heavy-ion collisions, $\langle\langle p_T \rangle\rangle$ is sensitive to the initial energy-to-entropy (E/S) ratio, $\langle p_T \rangle \propto E/S$ [23, 168], and typically decreases from central to peripheral collisions due to a reduced hydrodynamic response, as evident in Fig. 2.

The flow development in these collisions is governed primarily by two factors: the spatial homogeneity of the nuclear distribution and the compactness of the α clusters. Since the root-mean-square (RMS) radius of ^{16}O is fixed to its experimental value, the increase in cluster compactness from Cl. I to Cl. III necessarily leads to a corresponding increase in inter-cluster separation. In ultra-central collisions, the geometry of the overlap region reflects the overall shape of the nucleus, whereas in peripheral collisions, it is dominated by the geometry of the individual clusters.

As a result, in ultra-central collisions, increasing compactness and inter-cluster distance leads to reduced homogeneity and more localized sources of flow (hotspots), causing $\langle\langle p_T \rangle\rangle$ to decrease. In contrast, in peripheral collisions, the inter-cluster distance becomes less relevant, and greater compactness enhances $\langle\langle p_T \rangle\rangle$ due to larger E/S ratio of individual clusters.

B. Symmetric and Asymmetric Cumulants

In this section, we present our findings on the normalized symmetric $\text{NSC}(m, n)$ and asymmetric $\text{NAC}_{2,1}(m, n)$ cumulants obtained from our simulations. To evaluate their sensitivity to different nuclear configurations, we compared these observables for the nu-

clear configurations given in Table I, utilizing the two sets of ensembles detailed in Table III for TRENTo and TRENTo + MUSIC simulations. Negative values of $\text{NSC}(2, 3)$ throughout the centrality range reveal the anti-correlation between v_2 and v_3 . In contrast, $\text{NSC}(2, 4)$ is positive for all centralities, indicating positive correlations between v_2 and v_4 . Symmetric cumulants do not have contributions from non-flow effects, where non-flow refers to azimuthal correlations not related to the reaction plane orientation, like those from resonances, jets, quantum statistics, etc. This is verified by computing these observables for the HIJING model, which includes only non-flow physics, for which these are consistently zero [106]. We found a substantial sensitivity in symmetric and asymmetric cumulants to nuclear geometry which arises primarily from the characteristics of anisotropic flow, as these cumulants incorporate higher powers of flow coefficients. As discussed in the introduction, normalization serves to mitigate the influence of the magnitudes of v_m and v_n on the cumulants. Consequently, it reduces the incidental sensitivity of $\text{SC}(m, n)$ and $\text{AC}_{2,1}(m, n)$ to shear and bulk viscosities and to resonance decay and late-stage hadronic interactions. Therefore, we show only the results for normalized cumulants, i.e., $\text{NSC}(m, n)$ and $\text{NAC}_{2,1}(m, n)$.

Our results indicate that both $\text{NSC}(2, 3)$ and $\text{NSC}(2, 4)$ are significantly different for the different nuclear configurations. We showed in Ref. [169] that $\text{NSC}(2, 3)$ is particularly insensitive to the hydrodynamic transport coefficients (simulated by MUSIC) and the late-stage hadronic interactions (simulated by UrqMD) and thus is an excellent probe for the initial state of the heavy ion collisions. Here, we have shown that $\text{NSC}(2, 3)$ can be used to discriminate the different nuclear configurations in $^{16}\text{O}+^{16}\text{O}$ collisions, particularly in the ultra-central heavy ion collisions [170]. As shown in Fig. 3, $\text{NSC}(2, 3)$ in the initial state (i.e., correlations between ε_2 and ε_3 , shown by dashed lines), very well discriminates the Woods-Saxon (black dashed) and the three different tetrahedral α clustered nuclear configurations. In the ultra-central collisions, for example, 0-0.1% centrality class, Cl. I (dashed red), Cl. II (dashed green), and Cl. III (dashed blue) values for $\text{NSC}(2, 3)$ are enhanced by more than 100%, 300%, and 400% compared to that of Woods-Saxon, respectively. Similarly, $\text{NSC}(2, 3)$ in the final state (i.e., the correlations between v_2 and v_3 , shown by solid lines) is able to distinguish different initial states. In 0-1% centrality class, $\text{NSC}(2, 3)$ in the final state of Cl. I (red solid), Cl. II (green solid), and Cl. III (blue solid) are enhanced by about 37%, 98%, and 123% compared to Woods-Saxon, respectively. However, this clear distinction is lost as one approaches mid-central and peripheral collisions. This may be because, in small systems like $^{16}\text{O}+^{16}\text{O}$ there is insufficient flow in the mid-central and peripheral collisions as can be seen from suppression of $\langle\langle p_T \rangle\rangle$ at these centralities in Fig. 2. In heavy ion collisions, $\langle\langle p_T \rangle\rangle$ remains almost flat throughout all centrality classes [171, 172]. The bands around the final state re-

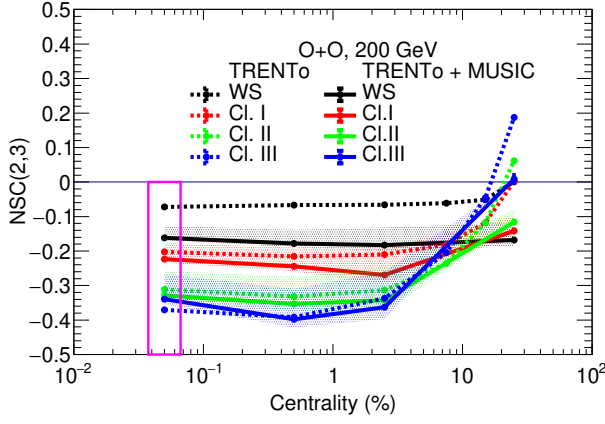


FIG. 3. Normalized symmetric cumulant vs centrality in $^{16}\text{O}+^{16}\text{O}$ collisions at $\sqrt{s_{NN}} = 200$ GeV. The shaded band represents the systematic uncertainties associated with η/s and ζ/s , with the dominant contribution arising from ζ/s and the influence of η/s being comparatively negligible. Dashed lines represent results from TRENTo, while solid lines correspond to the TRENTo+MUSIC framework. For TRENTo+MUSIC, $\text{NSC}(2,3)$ is consistently negative.

sults (solid lines) show systematic uncertainties due to shear and bulk viscosities. The major contribution to the systematics band is due to bulk viscosity and the influence of shear viscosity is negligible.

Similarly, $\text{NSC}(2,4)$, as shown in Fig. 4, can be used to distinguish between different nuclear configurations; however, it exhibits larger systematic uncertainties due to its sensitivity to shear and bulk viscosities, as well as to hadronic rescattering effects modeled by UrQMD [169]. The additional evolution through UrQMD may significantly modify the results, potentially diminishing the discriminatory power of this observable with respect to different nuclear configurations.

We now present the results for the asymmetric cumulants $\text{NAC}_{2,1}(m,n)$. In Fig. 5, we also illustrate the distinction among different nuclear configurations based on $\text{NAC}_{2,1}(2,3)$. We found that for $\text{NAC}_{2,1}(2,3)$, in the ultra-central collisions, for example, 0-0.1% centrality class, Cl. I (red dashed), Cl. II (green dashed), and Cl. III (blue dashed) values are enhanced by around 80%, 180%, and 230% compared to Woods-Saxon, respectively. This distinction arises from the initial state as can be seen from the large differences in the initial states values of $\text{NAC}_{2,1}(2,3)$. Again, this clear distinction is washed out as one approaches mid-central and peripheral collisions. The bands show the systematics due to shear and bulk viscosities. For $\text{NAC}_{2,1}(2,3)$, the narrow bands imply minuscule effect of both bulk and shear viscosity on this observable. This makes it even more effective than $\text{NSC}(2,3)$ to constraint the nuclear geometry of small nuclei like ^{16}O .

The influence of transport coefficients—specifically shear and bulk viscosities—as well as resonance decays and late-stage hadronic interactions, is particularly pro-

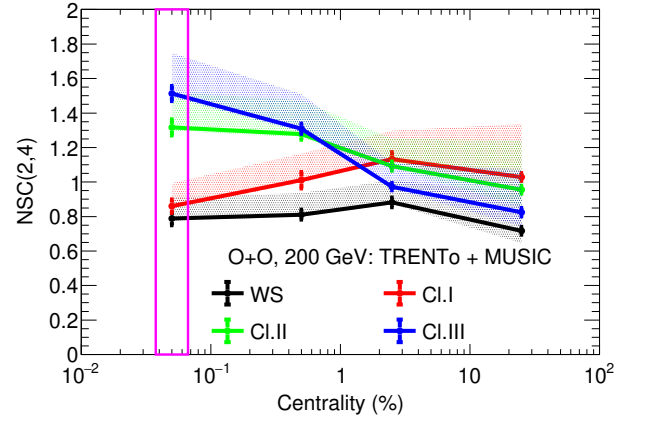


FIG. 4. Normalized symmetric cumulant vs centrality in $^{16}\text{O}+^{16}\text{O}$ collisions at $\sqrt{s_{NN}} = 200$ GeV for the TRENTo+MUSIC framework. The shaded band represents the systematic uncertainties associated with η/s and ζ/s , with the dominant contribution arising from ζ/s and the influence of η/s being comparatively smaller. $\text{NSC}(2,4)$ is consistently positive.

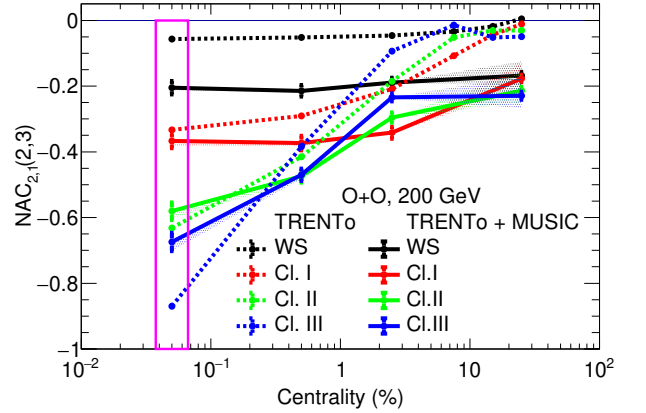


FIG. 5. Normalized asymmetric cumulant vs centrality in $^{16}\text{O}+^{16}\text{O}$ collisions at $\sqrt{s_{NN}} = 200$ GeV. The shaded bands represent systematic uncertainties associated with η/s and ζ/s , dominated by the latter in non-central collisions. $\text{NAC}_{2,1}(2,3)$ is consistently negative. Dashed lines represent results from TRENTo, while solid lines correspond to the TRENTo+MUSIC framework.

nounced for $\text{NAC}_{2,1}(2,4)$ [169]. This is reflected in Fig. 6, where the uncertainty bands are noticeably wider. While we are still able to distinguish between the Woods-Saxon and Cl. III configurations in the most ultra-central collisions, it is important to note that the inclusion of hadronic rescattering via UrQMD, which has not been applied in this analysis, may significantly alter the results and reduce the discriminatory power of $\text{NAC}_{2,1}(2,4)$ with respect to different nuclear configurations.

In Ref. [169], we showed the noteworthy similarities in the magnitude and centrality dependence of the normalized cumulants at RHIC and LHC. The comparison indicates minimal energy dependence for the normalized

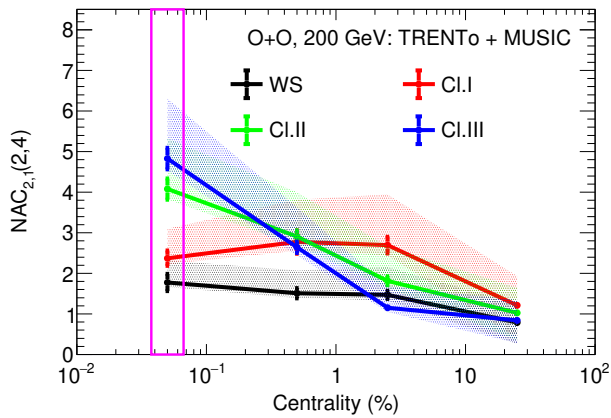


FIG. 6. Normalized asymmetric cumulant vs centrality in $^{16}\text{O}+^{16}\text{O}$ collisions at $\sqrt{s_{NN}} = 200$ GeV for the TRENTo+MUSIC framework. The shaded band represents the systematic uncertainties associated with η/s and ζ/s , with the dominant contribution arising from ζ/s and the influence of η/s being comparatively smaller. $\text{NAC}_{2,1}(2,4)$ is consistently positive.

cumulants. Therefore, our results are also applicable at LHC energies also.

As a result, the normalized symmetric and asymmetric cumulant measurements possess the capability to distinguish between diverse nuclear geometries, particularly within hydrodynamic and transport frameworks. $\text{NSC}(2,3)$ and $\text{NAC}_{2,1}(2,3)$, due to their insensitivity to hydrodynamic model parameters, resonance decay, and late-stage hadronic interactions, are especially valuable for constraining the initial conditions of the system's evolution.

C. v_1^{even}

In Fig. 7(a), we show how $\varepsilon_1\{2\}$ varies with centrality for different nuclear configurations. A clear hierarchy is observed among the clustered configurations, with the configuration featuring more compact clusters exhibiting larger $\varepsilon_1\{2\}$. This behavior arises because, as the clusters become more compact, the number of effective sources decreases, leading to larger fluctuations. To evaluate the sensitivity of v_1^{even} to different nuclear configurations, we compare its values for the configurations listed in Table I, using the first two parameter sets described in Table III, as shown in Fig. 7(c). Although $\varepsilon_1\{2\}$ increases from central to peripheral collisions, both the response ratio $v_1^{\text{even}}/\varepsilon_1\{2\}$, as shown in Fig. 7(b), and the mean transverse momentum $\langle p_T \rangle$, as shown in Fig. 2, decrease correspondingly, which explains the observed centrality dependence of v_1^{even} . We assessed the sensitivity of v_1^{even} to hadronic rescattering using UrQMD and observed negligible impact. Regarding the opposite hierarchy of v_1^{even} and the linear response across different clusters, two primary factors drive v_1^{even} : the initial dipole asymmetry,

ε_1 , and the hydrodynamic response of the QGP medium. Although ε_1 increases from Cl. I to Cl. III, the response (as well as $\langle p_T \rangle$) follows a decreasing trend. The dominance of ε_1 results in a similar hierarchy for v_1^{even} across the clusters. As the clustering becomes more compact, the magnitude of v_1^{even} increases. We observe substantial variation in v_1^{even} across different tetrahedral α -clustered O+O configurations, with a change of approximately 30% between the Woods-Saxon and Cl. III cases. This makes v_1^{even} a promising observable for distinguishing between Woods-Saxon and α -clustered nuclear geometries.

IV. CONCLUSIONS

We have presented results for multi-particle correlation functions in heavy-ion collisions at top RHIC energy using a hybrid framework based on TRENTo model, and MUSIC viscous hydrodynamics simulations.

First, we adjusted the free parameters, such as shear and bulk viscosities, to describe particle multiplicities, mean transverse momentum, and anisotropic flow for Au+Au collision system. After that, we discussed the impact of different nuclear geometries on the novel observables considering their sensitivities to shear and bulk viscosities, resonance decay, and hadronic interactions.

We have studied correlators that measure the correlations between flow harmonics of varying orders, including both symmetric and asymmetric cumulants as functions of centrality at midrapidity in $^{16}\text{O}+^{16}\text{O}$ collisions at $\sqrt{s_{NN}} = 200$ GeV. These observables are very sensitive to initial nuclear geometry. We found that $\text{NSC}(2,3)$ and in particular $\text{NAC}_{2,1}(2,3)$ being insensitive to both the hydro model parameters (shear and bulk viscosity) and late-stage hadronic interactions, are good observables for distinguishing different nuclear distributions in light nuclei like ^{16}O . This strongly supports their effectiveness as reliable tools for constraining the initial state of the system's evolution. Conversely, $\text{NSC}(2,4)$ and $\text{NAC}_{2,1}(2,4)$ exhibit considerable sensitivity to the hydrodynamic model parameters and to hadronic rescattering effects such as those modeled by UrQMD. Although in the absence of late-stage hadronic interactions these observables are capable of distinguishing between the Woods-Saxon and the most tetrahedral configurations in ultra-central collisions, the inclusion of such effects may significantly alter the results, potentially reducing their discriminatory power with respect to different nuclear configurations.

We observed an anticorrelation between the event-by-event fluctuations of v_2 and v_3 up to central collisions, while the fluctuations of v_2 and v_4 are found to be positively correlated. The observed anti-correlation between v_2 and v_3 appears to be driven by the initial-state anti-correlation between ε_2 and ε_3 , supporting the notion of linearity between ε_n and v_n [100]. This is consistent with the hydrodynamic picture in which final-state fluctuations originate from initial-state geometry. In contrast,

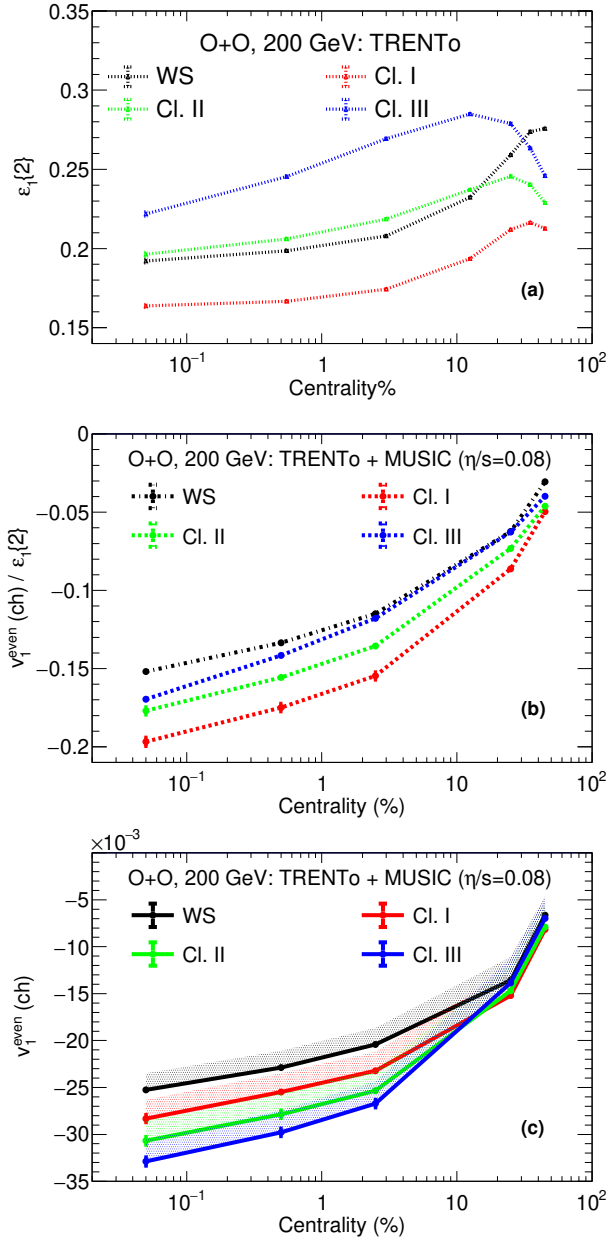


FIG. 7. Panel (a) shows $\varepsilon_1\{2\}$, panel (b) shows $v_1^{\text{even}}/\varepsilon_1\{2\}$ and panel (c) shows v_1^{even} in $^{16}\text{O}+^{16}\text{O}$ collisions at $\sqrt{s_{NN}} = 200$ GeV for the TRENTo+MUSIC framework. The shaded band for v_1^{even} represents the systematic uncertainties associated with η/s .

the correlation between v_2 and v_4 is primarily attributed to the nonlinear hydrodynamic response of the medium, as the linear component of the v_4 response is comparatively weaker.

In heavy-ion collisions, $\text{NSC}(m, n)$ measured by the STAR collaboration for Au+Au collisions at $\sqrt{s_{NN}} = 200$ GeV and the ALICE collaboration for Pb+Pb collisions at $\sqrt{s_{NN}} = 5.02$ TeV exhibit similar magnitudes and centrality trends. For $\text{NAC}_{2,1}(m, n)$, previous model results for Au+Au at $\sqrt{s_{NN}} = 200$ GeV showed behavior similar to the measurements made by ALICE. We anticipate comparable behavior in light-ion collisions, such as $^{16}\text{O} + ^{16}\text{O}$ collisions.

We also demonstrate that v_1^{even} proves to be a sensitive observable for distinguishing between Woods-Saxon and α -clustered nuclear geometries. The centrality dependence of v_1^{even} , explained by ε_1 and changes in the response ratio, $v_1^{\text{even}}/\varepsilon_1\{2\}$, and mean transverse momentum, $\langle\langle p_T \rangle\rangle$, reveals a clear trend from central to peripheral collisions. Moreover, substantial variation in v_1^{even} is observed across different tetrahedral α -clustered O+O configurations, with a notable 30% difference between Woods-Saxon and α -clustered distributions, with more compact clustering leading to an increased deviation from the Woods-Saxon nuclear geometry baseline. These findings highlight the potential of v_1^{even} as a tool for probing nuclear structure and geometry. Furthermore, we found that hadronic rescattering, as modeled by UrQMD, has a negligible impact on the final-state v_1^{even} signal.

V. ACKNOWLEDGEMENTS

We gratefully acknowledge Tribhuban Parida for the valuable discussions and for providing the computational setup, which played a crucial role in facilitating our analysis by enabling us to carry out extensive simulations and test various scenarios efficiently.

- [1] M. Bender, P.-H. Heenen, and P.-G. Reinhard, Self-consistent mean-field models for nuclear structure, *Rev. Mod. Phys.* **75**, 121 (2003).
- [2] K. Heyde and J. L. Wood, Shape coexistence in atomic nuclei, *Rev. Mod. Phys.* **83**, 1467 (2011).
- [3] P. Möller, A. J. Sierk, T. Ichikawa, and H. Sagawa, Nuclear ground-state masses and deformations: FRDM(2012),

Atom. Data Nucl. Data Tabl. **109-110**, 1 (2016), arXiv:1508.06294 [nucl-th].

- [4] F. Close, *Nuclear Physics: A Very Short Introduction*, Very short introductions (Oxford University Press, 2015).
- [5] J. P. Delaroche, M. Girod, J. Libert, H. Goutte, S. Hilaire, S. Peru, N. Pillet, and G. F. Bertsch, Structure of even-even nuclei using a mapped

- collective Hamiltonian and the D1S Gogny interaction, *Phys. Rev. C* **81**, 014303 (2010), arXiv:0910.2940 [nucl-th].
- [6] P. Y. Wang, J. G. Li, S. Zhang, Q. Yuan, M. R. Xie, and W. Zuo, Ab initio calculations with a new local chiral N3LO nucleon-nucleon force, *Phys. Rev. C* **109**, 064316 (2024), arXiv:2406.07956 [nucl-th].
- [7] A. Demyanova, A. Danilov, V. Starastsin, S. Goncharov, and T. Leonova, Search for states with enhanced radii in ^{20}Ne , *AIP Conf. Proc.* **3020**, 020001 (2024).
- [8] S. Hamada, A. H. Al-Ghamdi, A. A. Alholaisi, A. A. Ibraheem, N. Amangeldi, and Y. Abdou, Analysis of elastic scattering of $6,7\text{Li}$ and ^{20}Ne from ^{24}Mg nucleus using microscopic potentials, *Int. J. Mod. Phys. E* **32**, 2350015 (2023).
- [9] L. Morales-Gallegos *et al.*, Direct measurements of the $^{12}\text{C}(^{12}\text{C},p)^{23}\text{Na}$ and $^{12}\text{C}(^{12}\text{C},\alpha)^{20}\text{Ne}$ reactions at low energies for Nuclear Astrophysics, *EPJ Web Conf.* **260**, 01006 (2022).
- [10] D. Kekejian, *Deformed No-Core Shell Model and Symplectic Effective Field Theory*, Ph.D. thesis, Louisiana State U. (2022).
- [11] X. F. Yang, S. J. Wang, S. G. Wilkins, and R. F. Garcia Ruiz, Laser spectroscopy for the study of exotic nuclei, *Prog. Part. Nucl. Phys.* **129**, 104005 (2023), arXiv:2209.15228 [nucl-ex].
- [12] N. Magdy, M. Hegazy, A. Rafaat, W. Li, A. Deshpande, A. M. H. Abdelhady, A. Y. Ellithi, R. A. Lacey, and Z. Tu, A study of nuclear structure of light nuclei at the electron-ion collider, *Eur. Phys. J. A* **60**, 212 (2024), arXiv:2405.07844 [nucl-th].
- [13] D. Cline, Nuclear shapes studied by coulomb excitation, *Ann. Rev. Nucl. Part. Sci.* **36**, 683 (1986).
- [14] U.-G. Meißner, A new tool in nuclear physics: Nuclear lattice simulations, *Nucl. Phys. News.* **24**, 11 (2014), arXiv:1505.06997 [nucl-th].
- [15] S. Elhatisari, E. Epelbaum, H. Krebs, T. A. Lähde, D. Lee, N. Li, B.-n. Lu, U.-G. Meißner, and G. Rupak, Ab initio Calculations of the Isotopic Dependence of Nuclear Clustering, *Phys. Rev. Lett.* **119**, 222505 (2017), arXiv:1702.05177 [nucl-th].
- [16] M. Frosini, T. Duguet, J.-P. Ebran, and V. Somà, Multi-reference many-body perturbation theory for nuclei: I. Novel PGCM-PT formalism, *Eur. Phys. J. A* **58**, 62 (2022), arXiv:2110.15737 [nucl-th].
- [17] M. Frosini, T. Duguet, J.-P. Ebran, B. Bally, T. Mongelli, T. R. Rodríguez, R. Roth, and V. Somà, Multi-reference many-body perturbation theory for nuclei: II. Ab initio study of neon isotopes via PGCM and IM-NCSM calculations, *Eur. Phys. J. A* **58**, 63 (2022), arXiv:2111.00797 [nucl-th].
- [18] M. Frosini, T. Duguet, J.-P. Ebran, B. Bally, H. Hergert, T. R. Rodríguez, R. Roth, J. Yao, and V. Somà, Multi-reference many-body perturbation theory for nuclei: III. Ab initio calculations at second order in PGCM-PT, *Eur. Phys. J. A* **58**, 64 (2022), arXiv:2111.01461 [nucl-th].
- [19] D. Lonardonì, S. Gandolfi, J. E. Lynn, C. Petrie, J. Carlson, K. E. Schmidt, and A. Schwenk, Auxiliary field diffusion Monte Carlo calculations of light and medium-mass nuclei with local chiral interactions, *Phys. Rev. C* **97**, 044318 (2018), arXiv:1802.08932 [nucl-th].
- [20] W. Busza, K. Rajagopal, and W. van der Schee, Heavy Ion Collisions: The Big Picture, and the Big Questions, *Ann. Rev. Nucl. Part. Sci.* **68**, 339 (2018), arXiv:1802.04801 [hep-ph].
- [21] D. A. Teaney, Viscous Hydrodynamics and the Quark Gluon Plasma, in *Quark-gluon plasma 4*, edited by R. C. Hwa and X.-N. Wang (2010) pp. 207–266, arXiv:0905.2433 [nucl-th].
- [22] J.-Y. Ollitrault, Measures of azimuthal anisotropy in high-energy collisions, *Eur. Phys. J. A* **59**, 236 (2023), arXiv:2308.11674 [nucl-ex].
- [23] D. Teaney and L. Yan, Triangularity and Dipole Asymmetry in Heavy Ion Collisions, *Phys. Rev. C* **83**, 064904 (2011), arXiv:1010.1876 [nucl-th].
- [24] I. Arsene *et al.* (BRAHMS), Quark gluon plasma and color glass condensate at RHIC? The Perspective from the BRAHMS experiment, *Nucl. Phys. A* **757**, 1 (2005), arXiv:nucl-ex/0410020.
- [25] B. B. Back *et al.* (PHOBOS), The PHOBOS perspective on discoveries at RHIC, *Nucl. Phys. A* **757**, 28 (2005), arXiv:nucl-ex/0410022.
- [26] J. Adams *et al.* (STAR), Experimental and theoretical challenges in the search for the quark gluon plasma: The STAR Collaboration's critical assessment of the evidence from RHIC collisions, *Nucl. Phys. A* **757**, 102 (2005), arXiv:nucl-ex/0501009.
- [27] K. Adcox *et al.* (PHENIX), Formation of dense partonic matter in relativistic nucleus-nucleus collisions at RHIC: Experimental evaluation by the PHENIX collaboration, *Nucl. Phys. A* **757**, 184 (2005), arXiv:nucl-ex/0410003.
- [28] J. Adam *et al.* (ALICE), Enhanced production of multi-strange hadrons in high-multiplicity proton-proton collisions, *Nature Phys.* **13**, 535 (2017), arXiv:1606.07424 [nucl-ex].
- [29] V. Khachatryan *et al.* (CMS), Evidence for collectivity in pp collisions at the LHC, *Phys. Lett. B* **765**, 193 (2017), arXiv:1606.06198 [nucl-ex].
- [30] U. Heinz and R. Snellings, Collective flow and viscosity in relativistic heavy-ion collisions, *Ann. Rev. Nucl. Part. Sci.* **63**, 123 (2013), arXiv:1301.2826 [nucl-th].
- [31] P. Romatschke and U. Romatschke, *Relativistic Fluid Dynamics In and Out of Equilibrium*, Cambridge Monographs on Mathematical Physics (Cambridge University Press, 2019) arXiv:1712.05815 [nucl-th].
- [32] J. Berges, M. P. Heller, A. Mazeliauskas, and R. Venugopalan, QCD thermalization: Ab initio approaches and interdisciplinary connections, *Rev. Mod. Phys.* **93**, 035003 (2021), arXiv:2005.12299 [hep-th].
- [33] L. Adamczyk *et al.* (STAR), Elliptic flow of identified hadrons in Au+Au collisions at $\sqrt{s_{NN}} = 7.7\text{--}62.4$ GeV, *Phys. Rev. C* **88**, 014902 (2013), arXiv:1301.2348 [nucl-ex].
- [34] L. Adamczyk *et al.* (STAR), Beam-Energy Dependence of the Directed Flow of Protons, Antiprotons, and Pions in Au+Au Collisions, *Phys. Rev. Lett.* **112**, 162301 (2014), arXiv:1401.3043 [nucl-ex].

- [35] L. Adamczyk *et al.* (STAR), Third Harmonic Flow of Charged Particles in Au+Au Collisions at $\sqrt{s_{NN}} = 200$ GeV, *Phys. Rev. C* **88**, 014904 (2013), arXiv:1301.2187 [nucl-ex].
- [36] L. Adamczyk *et al.* (STAR), Observation of charge asymmetry dependence of pion elliptic flow and the possible chiral magnetic wave in heavy-ion collisions, *Phys. Rev. Lett.* **114**, 252302 (2015), arXiv:1504.02175 [nucl-ex].
- [37] W. Broniowski and E. Ruiz Arriola, Signatures of α Clustering in Light Nuclei from Relativistic Nuclear Collisions, *Phys. Rev. Lett.* **112**, 112501 (2014), arXiv:1312.0289 [nucl-th].
- [38] Y.-A. Li, S. Zhang, and Y.-G. Ma, Signatures of α -clustering in ^{16}O by using a multiphase transport model, *Phys. Rev. C* **102**, 054907 (2020), arXiv:2010.10003 [hep-ph].
- [39] M. Rybczyński, M. Piotrowska, and W. Broniowski, Signatures of α clustering in ultrarelativistic collisions with light nuclei, *Phys. Rev. C* **97**, 034912 (2018), arXiv:1711.00438 [nucl-th].
- [40] S. Prasad, N. Mallick, R. Sahoo, and G. G. Barnaföldi, Anisotropic flow fluctuation as a possible signature of clustered nuclear geometry in O-O collisions at the Large Hadron Collider, *Phys. Lett. B* **860**, 139145 (2025), arXiv:2407.15065 [nucl-th].
- [41] D. Behera, S. Prasad, N. Mallick, and R. Sahoo, Effects of clustered nuclear geometry on the anisotropic flow in O-O collisions at the LHC within a multiphase transport model framework, *Phys. Rev. D* **108**, 054022 (2023), arXiv:2304.10879 [hep-ph].
- [42] J. He, W.-B. He, Y.-G. Ma, and S. Zhang, Machine-learning-based identification for initial clustering structure in relativistic heavy-ion collisions, *Phys. Rev. C* **104**, 044902 (2021), arXiv:2109.06277 [hep-ph].
- [43] P. Bozek, W. Broniowski, E. Ruiz Arriola, and M. Rybczynski, α clusters and collective flow in ultrarelativistic carbon-heavy-nucleus collisions, *Phys. Rev. C* **90**, 064902 (2014), arXiv:1410.7434 [nucl-th].
- [44] N. Summerfield, B.-N. Lu, C. Plumberg, D. Lee, J. Noronha-Hostler, and A. Timmins, ^{16}O ^{16}O collisions at energies available at the BNL Relativistic Heavy Ion Collider and at the CERN Large Hadron Collider comparing α clustering versus substructure, *Phys. Rev. C* **104**, L041901 (2021), arXiv:2103.03345 [nucl-th].
- [45] C. Ding, L.-G. Pang, S. Zhang, and Y.-G. Ma, Signals of α clusters in $^{16}\text{O}+^{16}\text{O}$ collisions at the LHC from relativistic hydrodynamic simulations, *Chin. Phys. C* **47**, 024105 (2023).
- [46] Y.-Z. Wang, S. Zhang, and Y.-G. Ma, System dependence of away-side broadening and α -clustering light nuclei structure effect in dihadron azimuthal correlations, *Phys. Lett. B* **831**, 137198 (2022), arXiv:2112.08617 [nucl-th].
- [47] Z. Lu, M. Zhao, E. G. D. Nielsen, X. Li, and Y. Zhou, Signature of the α -clustering structure of Light Nuclei in Relativistic Nuclear Collisions, (2025), arXiv:2501.14852 [nucl-th].
- [48] S. H. Lim, J. Carlson, C. Loizides, D. Lonardoni, J. E. Lynn, J. L. Nagle, J. D. Orjuela Koop, and J. Ouellette, Exploring New Small System Geometries in Heavy Ion Collisions, *Phys. Rev. C* **99**, 044904 (2019), arXiv:1812.08096 [nucl-th].
- [49] M. Rybczyński and W. Broniowski, Glauber Monte Carlo predictions for ultrarelativistic collisions with ^{16}O , *Phys. Rev. C* **100**, 064912 (2019), arXiv:1910.09489 [hep-ph].
- [50] L.-M. Liu, S.-J. Li, Z. Wang, J. Xu, Z.-Z. Ren, and X.-G. Huang, Probing configuration of α clusters with spectator particles in relativistic heavy-ion collisions, *Phys. Lett. B* **854**, 138724 (2024), arXiv:2312.13572 [nucl-th].
- [51] G. Giacalone *et al.*, The unexpected uses of a bowling pin: exploiting ^{20}Ne isotopes for precision characterizations of collectivity in small systems, (2024), arXiv:2402.05995 [nucl-th].
- [52] L. Adamczyk *et al.* (STAR), Beam-energy-dependent two-pion interferometry and the freeze-out eccentricity of pions measured in heavy ion collisions at the STAR detector, *Phys. Rev. C* **92**, 014904 (2015), arXiv:1403.4972 [nucl-ex].
- [53] R. A. Lacey, Indications for a Critical End Point in the Phase Diagram for Hot and Dense Nuclear Matter, *Phys. Rev. Lett.* **114**, 142301 (2015), arXiv:1411.7931 [nucl-ex].
- [54] A. Adare *et al.* (PHENIX), Beam-energy and system-size dependence of the space-time extent of the pion emission source produced in heavy ion collisions, (2014), arXiv:1410.2559 [nucl-ex].
- [55] N. M. Abdelwahab *et al.* (STAR), Energy Dependence of K/π , p/π , and K/p Fluctuations in Au+Au Collisions from $\sqrt{s_{NN}} = 7.7$ to 200 GeV, *Phys. Rev. C* **92**, 021901 (2015), arXiv:1410.5375 [nucl-ex].
- [56] X. Luo and N. Xu, Search for the QCD Critical Point with Fluctuations of Conserved Quantities in Relativistic Heavy-Ion Collisions at RHIC : An Overview, *Nucl. Sci. Tech.* **28**, 112 (2017), arXiv:1701.02105 [nucl-ex].
- [57] M. I. Abdulhamid *et al.* (STAR), Imaging shapes of atomic nuclei in high-energy nuclear collisions, *Nature* **635**, 67 (2024), arXiv:2401.06625 [nucl-ex].
- [58] G. Giacalone, G. Nijs, and W. van der Schee, Determination of the Neutron Skin of Pb208 from Ultrarelativistic Nuclear Collisions, *Phys. Rev. Lett.* **131**, 202302 (2023), arXiv:2305.00015 [nucl-th].
- [59] H. Mäntysaari, B. Schenke, C. Shen, and W. Zhao, Multiscale Imaging of Nuclear Deformation at the Electron-Ion Collider, *Phys. Rev. Lett.* **131**, 062301 (2023), arXiv:2303.04866 [nucl-th].
- [60] M. Abdallah *et al.* (STAR), Search for the chiral magnetic effect with isobar collisions at $\sqrt{s_{NN}}=200$ GeV by the STAR Collaboration at the BNL Relativistic Heavy Ion Collider, *Phys. Rev. C* **105**, 014901 (2022), arXiv:2109.00131 [nucl-ex].
- [61] G. Giacalone, *A matter of shape: seeing the deformation of atomic nuclei at high-energy colliders*, Ph.D. thesis, U. Paris-Saclay (2020), arXiv:2101.00168 [nucl-th].
- [62] P. Filip, R. Lednicky, H. Masui, and N. Xu, Initial eccentricity in deformed Au-197 + Au-197 and U-238 + U-238 collisions at $s_{NN}=200$ GeV at the BNL Relativistic Heavy Ion Collider, *Phys. Rev. C* **80**, 054903 (2009).

- [63] Q. Y. Shou, Y. G. Ma, P. Sorensen, A. H. Tang, F. Videbæk, and H. Wang, Parameterization of Deformed Nuclei for Glauber Modeling in Relativistic Heavy Ion Collisions, *Phys. Lett. B* **749**, 215 (2015), arXiv:1409.8375 [nucl-th].
- [64] G. Giacalone, Observing the deformation of nuclei with relativistic nuclear collisions, *Phys. Rev. Lett.* **124**, 202301 (2020), arXiv:1910.04673 [nucl-th].
- [65] C. Zhang and J. Jia, Evidence of Quadrupole and Octupole Deformations in Zr96+Zr96 and Ru96+Ru96 Collisions at Ultrarelativistic Energies, *Phys. Rev. Lett.* **128**, 022301 (2022), arXiv:2109.01631 [nucl-th].
- [66] H. Li, H.-j. Xu, Y. Zhou, X. Wang, J. Zhao, L.-W. Chen, and F. Wang, Probing the neutron skin with ultrarelativistic isobaric collisions, *Phys. Rev. Lett.* **125**, 222301 (2020), arXiv:1910.06170 [nucl-th].
- [67] L.-M. Liu, C.-J. Zhang, J. Zhou, J. Xu, J. Jia, and G.-X. Peng, Probing neutron-skin thickness with free spectator neutrons in ultracentral high-energy isobaric collisions, *Phys. Lett. B* **834**, 137441 (2022), arXiv:2203.09924 [nucl-th].
- [68] F. G. Gardim, F. Grassi, M. Luzum, and J.-Y. Ollitrault, Mapping the hydrodynamic response to the initial geometry in heavy-ion collisions, *Phys. Rev. C* **85**, 024908 (2012), arXiv:1111.6538 [nucl-th].
- [69] H. Niemi, G. S. Denicol, H. Holopainen, and P. Huovinen, Event-by-event distributions of azimuthal asymmetries in ultrarelativistic heavy-ion collisions, *Phys. Rev. C* **87**, 054901 (2013), arXiv:1212.1008 [nucl-th].
- [70] D. Teaney and L. Yan, Non linearities in the harmonic spectrum of heavy ion collisions with ideal and viscous hydrodynamics, *Phys. Rev. C* **86**, 044908 (2012), arXiv:1206.1905 [nucl-th].
- [71] Z. Qiu and U. W. Heinz, Event-by-event shape and flow fluctuations of relativistic heavy-ion collision fireballs, *Phys. Rev. C* **84**, 024911 (2011), arXiv:1104.0650 [nucl-th].
- [72] F. G. Gardim, J. Noronha-Hostler, M. Luzum, and F. Grassi, Effects of viscosity on the mapping of initial to final state in heavy ion collisions, *Phys. Rev. C* **91**, 034902 (2015), arXiv:1411.2574 [nucl-th].
- [73] B. Betz, M. Gyulassy, M. Luzum, J. Noronha, J. Noronha-Hostler, I. Portillo, and C. Ratti, Cumulants and nonlinear response of high p_T harmonic flow at $\sqrt{s_{NN}} = 5.02$ TeV, *Phys. Rev. C* **95**, 044901 (2017), arXiv:1609.05171 [nucl-th].
- [74] S. Rao, M. Sievert, and J. Noronha-Hostler, Baseline predictions of elliptic flow and fluctuations for the RHIC Beam Energy Scan using response coefficients, *Phys. Rev. C* **103**, 034910 (2021), arXiv:1910.03677 [nucl-th].
- [75] M. Hippert, J. a. G. P. Barbon, D. Dobrigkeit Chinelato, M. Luzum, J. Noronha, T. Nunes da Silva, W. M. Serenone, and J. Takahashi, Probing the structure of the initial state of heavy-ion collisions with p_T -dependent flow fluctuations, *Phys. Rev. C* **102**, 064909 (2020), arXiv:2006.13358 [nucl-th].
- [76] A. Bilandzic, R. Snellings, and S. Voloshin, Flow analysis with cumulants: Direct calculations, *Phys. Rev. C* **83**, 044913 (2011), arXiv:1010.0233 [nucl-ex].
- [77] M. Luzum and H. Petersen, Initial State Fluctuations and Final State Correlations in Relativistic Heavy-Ion Collisions, *J. Phys. G* **41**, 063102 (2014), arXiv:1312.5503 [nucl-th].
- [78] Y. Zhou, Review of anisotropic flow correlations in ultrarelativistic heavy-ion collisions, *Adv. High Energy Phys.* **2016**, 9365637 (2016), arXiv:1607.05613 [nucl-ex].
- [79] C. A. G. Prado, J. Noronha-Hostler, R. Katz, A. A. P. Suaide, J. Noronha, M. G. Munhoz, and M. R. Cosentino, Event-by-event correlations between soft hadrons and D^0 mesons in 5.02 TeV PbPb collisions at the CERN Large Hadron Collider, *Phys. Rev. C* **96**, 064903 (2017), arXiv:1611.02965 [nucl-th].
- [80] S. Acharya *et al.* (ALICE), Event-shape engineering for the D-meson elliptic flow in mid-central Pb-Pb collisions at $\sqrt{s_{NN}} = 5.02$ TeV, *JHEP* **02**, 150, arXiv:1809.09371 [nucl-ex].
- [81] J. Noronha-Hostler, L. Yan, F. G. Gardim, and J.-Y. Ollitrault, Linear and cubic response to the initial eccentricity in heavy-ion collisions, *Phys. Rev. C* **93**, 014909 (2016), arXiv:1511.03896 [nucl-th].
- [82] H. Niemi, K. J. Eskola, R. Paatelainen, and K. Tuominen, Predictions for 5.023 TeV Pb + Pb collisions at the CERN Large Hadron Collider, *Phys. Rev. C* **93**, 014912 (2016), arXiv:1511.04296 [hep-ph].
- [83] J. Adam *et al.* (ALICE), Centrality Dependence of the Charged-Particle Multiplicity Density at Midrapidity in Pb-Pb Collisions at $\sqrt{s_{NN}} = 5.02$ TeV, *Phys. Rev. Lett.* **116**, 222302 (2016), arXiv:1512.06104 [nucl-ex].
- [84] J. E. Bernhard, J. S. Moreland, and S. A. Bass, Bayesian estimation of the specific shear and bulk viscosity of quark-gluon plasma, *Nature Phys.* **15**, 1113 (2019).
- [85] C. Shen and L. Yan, Recent development of hydrodynamic modeling in heavy-ion collisions, *Nucl. Sci. Tech.* **31**, 122 (2020), arXiv:2010.12377 [nucl-th].
- [86] P. Braun-Munzinger, V. Koch, T. Schäfer, and J. Stachel, Properties of hot and dense matter from relativistic heavy ion collisions, *Phys. Rept.* **621**, 76 (2016), arXiv:1510.00442 [nucl-th].
- [87] S. Voloshin and Y. Zhang, Flow study in relativistic nuclear collisions by Fourier expansion of Azimuthal particle distributions, *Z. Phys. C* **70**, 665 (1996), arXiv:hep-ph/9407282.
- [88] J.-Y. Ollitrault, Anisotropy as a signature of transverse collective flow, *Phys. Rev. D* **46**, 229 (1992).
- [89] S. A. Bass, M. Gyulassy, H. Stoecker, and W. Greiner, Signatures of quark gluon plasma formation in high-energy heavy ion collisions: A Critical review, *J. Phys. G* **25**, R1 (1999), arXiv:hep-ph/9810281.
- [90] S. A. Voloshin, A. M. Poskanzer, and R. Snellings, Collective phenomena in non-central nuclear collisions, *Landolt-Bornstein* **23**, 293 (2010), arXiv:0809.2949 [nucl-ex].

- [91] S. A. Voloshin and A. M. Poskanzer, The Physics of the centrality dependence of elliptic flow, *Phys. Lett. B* **474**, 27 (2000), arXiv:nucl-th/9906075.
- [92] Y. B. Ivanov and A. A. Soldatov, Elliptic Flow in Heavy-Ion Collisions at Energies $\sqrt{s_{NN}} = 2.7\text{--}39$ GeV, *Phys. Rev. C* **91**, 024914 (2015), arXiv:1401.2265 [nucl-th].
- [93] J. Adams *et al.* (STAR), Azimuthal anisotropy in Au+Au collisions at $s(NN)^{1/2} = 200\text{--}600$ GeV, *Phys. Rev. C* **72**, 014904 (2005), arXiv:nucl-ex/0409033.
- [94] C. Adler *et al.* (STAR), Identified particle elliptic flow in Au + Au collisions at $s(NN)^{1/2} = 130\text{--}600$ GeV, *Phys. Rev. Lett.* **87**, 182301 (2001), arXiv:nucl-ex/0107003.
- [95] K. Aamodt *et al.* (ALICE), Elliptic flow of charged particles in Pb-Pb collisions at 2.76 TeV, *Phys. Rev. Lett.* **105**, 252302 (2010), arXiv:1011.3914 [nucl-ex].
- [96] H. Sorge, Highly sensitive centrality dependence of elliptic flow: A novel signature of the phase transition in QCD, *Phys. Rev. Lett.* **82**, 2048 (1999), arXiv:nucl-th/9812057.
- [97] D. Solanki, P. Sorensen, S. Basu, R. Raniwala, and T. K. Nayak, Beam energy dependence of Elliptic and Triangular flow with the AMPT model, *Phys. Lett. B* **720**, 352 (2013), arXiv:1210.0512 [nucl-ex].
- [98] J. Adam *et al.* (ALICE), Higher harmonic flow coefficients of identified hadrons in Pb-Pb collisions at $\sqrt{s_{NN}} = 2.76$ TeV, *JHEP* **09**, 164, arXiv:1606.06057 [nucl-ex].
- [99] U. Heinz, Z. Qiu, and C. Shen, Fluctuating flow angles and anisotropic flow measurements, *Phys. Rev. C* **87**, 034913 (2013), arXiv:1302.3535 [nucl-th].
- [100] B. Alver and G. Roland, Collision geometry fluctuations and triangular flow in heavy-ion collisions, *Phys. Rev. C* **81**, 054905 (2010), [Erratum: *Phys. Rev. C* **82**, 039903 (2010)], arXiv:1003.0194 [nucl-th].
- [101] J. E. Parkkila, A. Onnerstad, and D. J. Kim, Bayesian estimation of the specific shear and bulk viscosity of the quark-gluon plasma with additional flow harmonic observables, *Phys. Rev. C* **104**, 054904 (2021), arXiv:2106.05019 [hep-ph].
- [102] E. Retinskaya, M. Luzum, and J.-Y. Ollitrault, Constraining models of initial state with v_2 and v_3 data from LHC and RHIC, *Nucl. Phys. A* **926**, 152 (2014), arXiv:1401.3241 [nucl-th].
- [103] C. Shen and U. Heinz, Collision Energy Dependence of Viscous Hydrodynamic Flow in Relativistic Heavy-Ion Collisions, *Phys. Rev. C* **85**, 054902 (2012), [Erratum: *Phys. Rev. C* **86**, 049903 (2012)], arXiv:1202.6620 [nucl-th].
- [104] D. Teaney, The Effects of viscosity on spectra, elliptic flow, and HBT radii, *Phys. Rev. C* **68**, 034913 (2003), arXiv:nucl-th/0301099.
- [105] C. Shen, S. A. Bass, T. Hirano, P. Huovinen, Z. Qiu, H. Song, and U. Heinz, The QGP shear viscosity: Elusive goal or just around the corner?, *J. Phys. G* **38**, 124045 (2011), arXiv:1106.6350 [nucl-th].
- [106] A. Bilandzic, M. Lesch, C. Mordasini, and S. F. Taghavi, Multivariate cumulants in flow analyses: The next generation, *Phys. Rev. C* **105**, 024912 (2022).
- [107] A. Bilandzic, C. H. Christensen, K. Gulbrandsen, A. Hansen, and Y. Zhou, Generic framework for anisotropic flow analyses with multiparticle azimuthal correlations, *Phys. Rev. C* **89**, 064904 (2014), arXiv:1312.3572 [nucl-ex].
- [108] C. Mordasini, A. Bilandzic, D. Karakoç, and S. F. Taghavi, Higher order Symmetric Cumulants, *Phys. Rev. C* **102**, 024907 (2020), arXiv:1901.06968 [nucl-ex].
- [109] S. Acharya *et al.* (ALICE), Systematic studies of correlations between different order flow harmonics in Pb-Pb collisions at $\sqrt{s_{NN}} = 2.76$ TeV, *Phys. Rev. C* **97**, 024906 (2018), arXiv:1709.01127 [nucl-ex].
- [110] S. F. Taghavi, A Fourier-cumulant analysis for multiharmonic flow fluctuation: by employing a multidimensional generating function approach, *Eur. Phys. J. C* **81**, 652 (2021), arXiv:2005.04742 [nucl-th].
- [111] X. Zhu, Y. Zhou, H. Xu, and H. Song, Correlations of flow harmonics in 2.76A TeV Pb-Pb collisions, *Phys. Rev. C* **95**, 044902 (2017), arXiv:1608.05305 [nucl-th].
- [112] B. Schenke, C. Shen, and P. Tribedy, Multi-particle and charge-dependent azimuthal correlations in heavy-ion collisions at the Relativistic Heavy-Ion Collider, *Phys. Rev. C* **99**, 044908 (2019), arXiv:1901.04378 [nucl-th].
- [113] H. Hirvonen, K. J. Eskola, and H. Niemi, Flow correlations from a hydrodynamics model with dynamical freeze-out and initial conditions based on perturbative QCD and saturation, *Phys. Rev. C* **106**, 044913 (2022), arXiv:2206.15207 [hep-ph].
- [114] N. Magdy, Characterizing initial- and final-state effects of relativistic nuclear collisions, *Phys. Rev. C* **107**, 024905 (2023), arXiv:2210.14091 [nucl-th].
- [115] N. Magdy, Characterizing the initial- and final-state effects in isobaric collisions at energies available at the BNL Relativistic Heavy Ion Collider, *Phys. Rev. C* **109**, 024906 (2024), arXiv:2401.04083 [nucl-th].
- [116] F. G. Gardim, F. Grassi, M. Luzum, and J. Noronha-Hostler, Hydrodynamic Predictions for Mixed Harmonic Correlations in 200 GeV Au+Au Collisions, *Phys. Rev. C* **95**, 034901 (2017), arXiv:1608.02982 [nucl-th].
- [117] M. Nasim, Systematic study of symmetric cumulants at $\sqrt{s_{NN}} = 200$ GeV in Au+Au collision using transport approach, *Phys. Rev. C* **95**, 034905 (2017), arXiv:1612.01066 [nucl-ex].
- [118] J. Adam *et al.* (STAR), Correlation measurements between flow harmonics in au+au collisions at rhic, *Physics Letters B* **783**, 459 (2018).
- [119] J. Adam *et al.* (ALICE), Correlated event-by-event fluctuations of flow harmonics in Pb-Pb collisions at $\sqrt{s_{NN}} = 2.76$ TeV, *Phys. Rev. Lett.* **117**, 182301 (2016), arXiv:1604.07663 [nucl-ex].
- [120] S. Acharya *et al.* (ALICE), Higher-order correlations between different moments of two flow amplitudes in Pb-Pb collisions at

- sNN=5.02 TeV, Phys. Rev. C **108**, 055203 (2023), arXiv:2303.13414 [nucl-ex].
- [121] M. Aaboud *et al.* (ATLAS), Correlated long-range mixed-harmonic fluctuations measured in pp , p +Pb and low-multiplicity Pb+Pb collisions with the ATLAS detector, Phys. Lett. B **789**, 444 (2019), arXiv:1807.02012 [nucl-ex].
 - [122] A. Ortiz (ALICE, ATLAS, CMS, LHCb), Particle production and flow-like effects in small systems, PoS LHCP2019, 091 (2019), arXiv:1909.03937 [hep-ex].
 - [123] A. M. Sirunyan *et al.* (CMS), Correlations of azimuthal anisotropy Fourier harmonics with subevent cumulants in p Pb collisions at $\sqrt{s_{NN}}=8.16$ TeV, Phys. Rev. C **103**, 014902 (2021), arXiv:1905.09935 [hep-ex].
 - [124] S. Acharya *et al.* (ALICE), Measurements of mixed harmonic cumulants in Pb–Pb collisions at $\sqrt{s_{NN}}=5.02$ TeV, Phys. Lett. B **818**, 136354 (2021), arXiv:2102.12180 [nucl-ex].
 - [125] F. G. Gardim, F. Grassi, Y. Hama, M. Luzum, and J.-Y. Ollitrault, Directed flow at mid-rapidity in event-by-event hydrodynamics, Phys. Rev. C **83**, 064901 (2011), arXiv:1103.4605 [nucl-th].
 - [126] J. Adams *et al.* (STAR), Azimuthal anisotropy at RHIC: The First and fourth harmonics, Phys. Rev. Lett. **92**, 062301 (2004), [Erratum: Phys.Rev.Lett. **127**, 069901 (2021)], arXiv:nucl-ex/0310029.
 - [127] C. Alt *et al.* (NA49), Directed and elliptic flow of charged pions and protons in Pb + Pb collisions at 40-A-GeV and 158-A-GeV, Phys. Rev. C **68**, 034903 (2003), arXiv:nucl-ex/0303001.
 - [128] J. Adams *et al.* (STAR), Directed flow in Au+Au collisions at $s(NN)^{1/2}=62$ -GeV, Phys. Rev. C **73**, 034903 (2006), arXiv:nucl-ex/0510053.
 - [129] B. B. Back *et al.* (PHOBOS), Energy dependence of directed flow over a wide range of pseudorapidity in Au + Au collisions at RHIC, Phys. Rev. Lett. **97**, 012301 (2006), arXiv:nucl-ex/0511045.
 - [130] B. I. Abelev *et al.* (STAR), System-size independence of directed flow at the Relativistic Heavy-Ion Collider, Phys. Rev. Lett. **101**, 252301 (2008), arXiv:0807.1518 [nucl-ex].
 - [131] B. Abelev *et al.* (ALICE), Directed Flow of Charged Particles at Midrapidity Relative to the Spectator Plane in Pb-Pb Collisions at $\sqrt{s_{NN}}=2.76$ TeV, Phys. Rev. Lett. **111**, 232302 (2013), arXiv:1306.4145 [nucl-ex].
 - [132] T. Parida, *Phenomenology of baryon dynamics with directed flow in relativistic heavy-ion collisions*, Other thesis (2025), arXiv:2505.06522 [nucl-th].
 - [133] T. Parida, S. Chatterjee, and S. Singha, Charge dependent directed flow splitting from baryon inhomogeneity and electromagnetic field, (2025), arXiv:2503.04660 [nucl-th].
 - [134] T. Parida, S. Chatterjee, and M. Nasim, Effect of hadronic interaction on the flow of K^0 , Phys. Rev. C **109**, 044905 (2024), arXiv:2312.06359 [nucl-th].
 - [135] T. Parida and S. Chatterjee, Baryon diffusion coefficient of the strongly interacting medium, (2023), arXiv:2305.10371 [nucl-th].
 - [136] T. Parida and S. Chatterjee, Baryon inhomogeneities driven charge dependent directed flow in heavy ion collisions, (2023), arXiv:2305.08806 [nucl-th].
 - [137] T. Parida and S. Chatterjee, Directed flow of light flavor hadrons for Au+Au collisions at $\sqrt{s_{NN}}=7.7$ -200 GeV, (2022), arXiv:2211.15659 [nucl-th].
 - [138] T. Parida and S. Chatterjee, Directed flow in a baryonic fireball, (2022), arXiv:2211.15729 [nucl-th].
 - [139] P. Bozek, W. Broniowski, and J. Moreira, Torqued fireballs in relativistic heavy-ion collisions, Phys. Rev. C **83**, 034911 (2011), arXiv:1011.3354 [nucl-th].
 - [140] P. Bozek, Event-by-event viscous hydrodynamics for Cu–Au collisions at $\sqrt{s_{NN}}=200$ GeV, Phys. Lett. B **717**, 287 (2012), arXiv:1208.1887 [nucl-th].
 - [141] M. Miller and R. Snellings, Eccentricity fluctuations and its possible effect on elliptic flow measurements, (2003), arXiv:nucl-ex/0312008.
 - [142] N. Borghini and J.-Y. Ollitrault, Momentum spectra, anisotropic flow, and ideal fluids, Phys. Lett. B **642**, 227 (2006), arXiv:nucl-th/0506045.
 - [143] P. Danielewicz and G. Odyniec, Transverse Momentum Analysis of Collective Motion in Relativistic Nuclear Collisions, Phys. Lett. B **157**, 146 (1985), arXiv:2109.05308 [nucl-th].
 - [144] A. M. Poskanzer and S. A. Voloshin, Methods for analyzing anisotropic flow in relativistic nuclear collisions, Phys. Rev. C **58**, 1671 (1998), arXiv:nucl-ex/9805001.
 - [145] M. Luzum and J.-Y. Ollitrault, Directed flow at midrapidity in heavy-ion collisions, Phys. Rev. Lett. **106**, 102301 (2011), arXiv:1011.6361 [nucl-ex].
 - [146] J. Jia (ATLAS), Measurement of the rapidity-even dipolar flow in Pb-Pb collisions with the ATLAS detector, J. Phys. Conf. Ser. **389**, 012013 (2012), arXiv:1208.1874 [nucl-ex].
 - [147] N. Borghini, P. M. Dinh, and J.-Y. Ollitrault, A New method for measuring azimuthal distributions in nucleus-nucleus collisions, Phys. Rev. C **63**, 054906 (2001), arXiv:nucl-th/0007063.
 - [148] E. Retinskaya, M. Luzum, and J.-Y. Ollitrault, Directed flow at midrapidity in $\sqrt{s_{NN}}=2.76$ TeV Pb+Pb collisions, Phys. Rev. Lett. **108**, 252302 (2012), arXiv:1203.0931 [nucl-th].
 - [149] M. Luzum and P. Romatschke, Conformal Relativistic Viscous Hydrodynamics: Applications to RHIC results at $s(NN)^{1/2}=200$ -GeV, Phys. Rev. C **78**, 034915 (2008), [Erratum: Phys.Rev.C **79**, 039903 (2009)], arXiv:0804.4015 [nucl-th].
 - [150] B. H. Alver, C. Gombeaud, M. Luzum, and J.-Y. Ollitrault, Triangular flow in hydrodynamics and transport theory, Phys. Rev. C **82**, 034913 (2010), arXiv:1007.5469 [nucl-th].
 - [151] B. Schenke, S. Jeon, and C. Gale, Higher flow harmonics from (3+1)D event-by-event viscous hydrodynamics, Phys. Rev. C **85**, 024901 (2012), arXiv:1109.6289 [hep-ph].
 - [152] N. Magdy and R. Lacey, Exploring rapidity-even dipolar flow in isobaric collisions at RHIC, J. Phys. G **51**, 09LT01 (2024),

- arXiv:2308.11031 [nucl-th].
- [153] J. Adam *et al.* (STAR), Beam energy dependence of rapidity-even dipolar flow in Au+Au collisions, *Phys. Lett. B* **784**, 26 (2018), arXiv:1804.08647 [nucl-ex].
 - [154] Y. Wang, S. Zhao, B. Cao, H.-j. Xu, and H. Song, Exploring the compactness of α clusters in O16 nuclei with relativistic O16+O16 collisions, *Phys. Rev. C* **109**, L051904 (2024), arXiv:2401.15723 [nucl-th].
 - [155] H. De Vries, C. W. De Jager, and C. De Vries, Nuclear charge and magnetization density distribution parameters from elastic electron scattering, *Atom. Data Nucl. Data Tabl.* **36**, 495 (1987).
 - [156] J. S. Moreland, J. E. Bernhard, and S. A. Bass, Bayesian calibration of a hybrid nuclear collision model using p-Pb and Pb-Pb data at energies available at the CERN Large Hadron Collider, *Phys. Rev. C* **101**, 024911 (2020), arXiv:1808.02106 [nucl-th].
 - [157] B. Schenke, S. Jeon, and C. Gale, (3+1)D hydrodynamic simulation of relativistic heavy-ion collisions, *Phys. Rev. C* **82**, 014903 (2010), arXiv:1004.1408 [hep-ph].
 - [158] B. Schenke, S. Jeon, and C. Gale, Elliptic and triangular flow in event-by-event (3+1)D viscous hydrodynamics, *Phys. Rev. Lett.* **106**, 042301 (2011), arXiv:1009.3244 [hep-ph].
 - [159] J.-F. Paquet, C. Shen, G. S. Denicol, M. Luzum, B. Schenke, S. Jeon, and C. Gale, Production of photons in relativistic heavy-ion collisions, *Phys. Rev. C* **93**, 044906 (2016), arXiv:1509.06738 [hep-ph].
 - [160] P. Huovinen and H. Petersen, Particlization in hybrid models, *Eur. Phys. J. A* **48**, 171 (2012), arXiv:1206.3371 [nucl-th].
 - [161] G. S. Denicol, T. Kodama, T. Koide, and P. Mota, Bulk viscosity effects on elliptic flow, *Nucl. Phys. A* **830**, 729C (2009), arXiv:0907.4269 [hep-ph].
 - [162] A. Monnai, B. Schenke, and C. Shen, Equation of state at finite densities for QCD matter in nuclear collisions, *Phys. Rev. C* **100**, 024907 (2019), arXiv:1902.05095 [nucl-th].
 - [163] A. Bazavov *et al.* (HotQCD), Equation of state in (2+1)-flavor QCD, *Phys. Rev. D* **90**, 094503 (2014), arXiv:1407.6387 [hep-lat].
 - [164] A. Bazavov *et al.* (HotQCD), Fluctuations and Correlations of net baryon number, electric charge, and strangeness: A comparison of lattice QCD results with the hadron resonance gas model, *Phys. Rev. D* **86**, 034509 (2012), arXiv:1203.0784 [hep-lat].
 - [165] H. T. Ding, S. Mukherjee, H. Ohno, P. Petreczky, and H. P. Schadler, Diagonal and off-diagonal quark number susceptibilities at high temperatures, *Phys. Rev. D* **92**, 074043 (2015), arXiv:1507.06637 [hep-lat].
 - [166] J. S. Moreland and R. A. Soltz, Hydrodynamic simulations of relativistic heavy-ion collisions with different lattice quantum chromodynamics calculations of the equation of state, *Phys. Rev. C* **93**, 044913 (2016), arXiv:1512.02189 [nucl-th].
 - [167] F. Cooper and G. Frye, Comment on the Single Particle Distribution in the Hydrodynamic and Statistical Thermodynamic Models of Multiparticle Production, *Phys. Rev. D* **10**, 186 (1974).
 - [168] G. Giacalone, F. G. Gardim, J. Noronha-Hostler, and J.-Y. Ollitrault, Correlation between mean transverse momentum and anisotropic flow in heavy-ion collisions, *Phys. Rev. C* **103**, 024909 (2021), arXiv:2004.01765 [nucl-th].
 - [169] K. Shafi, P. Dixit, S. Chatterjee, and M. Nasim, Exploring the flow harmonic correlations via multiparticle symmetric and asymmetric cumulants in Au+Au collisions at $\sqrt{s_{NN}} = 200$ GeV, (2024), arXiv:2405.02245 [nucl-th].
 - [170] P. Li, B. Zhou, and G.-L. Ma, Identifying α -cluster configurations in ^{20}Ne via ultracentral Ne+Ne Collisions, (2025), arXiv:2504.04688 [nucl-th].
 - [171] B. I. Abelev *et al.* (STAR), Systematic Measurements of Identified Particle Spectra in pp, d^+ Au and Au+Au Collisions from STAR, *Phys. Rev. C* **79**, 034909 (2009), arXiv:0808.2041 [nucl-ex].
 - [172] S. Acharya *et al.* (ALICE), Transverse momentum spectra and nuclear modification factors of charged particles in Xe-Xe collisions at $\sqrt{s_{NN}} = 5.44$ TeV, *Phys. Lett. B* **788**, 166 (2019), arXiv:1805.04399 [nucl-ex].